

Functional interplay between the cell cycle and cell phenotypes†

Cite this: *Integr. Biol.*, 2013, 5, 523

Wei-Chiang Chen,^{†,ab} Pei-Hsun Wu,^{†,ab} Jude M. Phillip,^{ab} Shyam B. Khatau,^{ab} Jae Min Choi,^b Matthew R. Dallas,^{ab} Konstantinos Konstantopoulos,^{ab} Sean X. Sun,^{ac} Jerry S. H. Lee,^{bd} Didier Hodzic^e and Denis Wirtz^{*ab}

Cell cycle distribution of adherent cells is typically assessed using flow cytometry, which precludes the measurements of many cell properties and their cycle phase in the same environment. Here we develop and validate a microscopy system to quantitatively analyze the cell-cycle phase of thousands of adherent cells and their associated cell properties simultaneously. This assay demonstrates that population-averaged cell phenotypes can be written as a linear combination of cell-cycle fractions and phase-dependent phenotypes. By perturbing the cell cycle through inhibition of cell-cycle regulators or changing nuclear morphology by depletion of structural proteins, our results reveal that cell cycle regulators and structural proteins can significantly interfere with each other's *prima facie* functions. This study introduces a high-throughput method to simultaneously measure the cell cycle and phenotypes at single-cell resolution, which reveals a complex functional interplay between the cell cycle and cell phenotypes.

Received 14th October 2012,
Accepted 5th December 2012

DOI: 10.1039/c2ib20246h

www.rsc.org/ibiology

Insight, innovation, integration

We demonstrate and validate a new high throughput microscopy-based method to measure properties of adherent cells (*e.g.*, nuclear and cell shape) and cell-cycle phases simultaneously, rapidly, and at single cell resolution. Without forced cell synchronization, this method shows and quantifies how cell phenotypes are strongly dependent on the cell cycle. Thanks to this single-cell method, we propose and validate a simple equation that quantitatively defines the separate contributions to changes in population-averaged phenotypes from cell-cycle changes and intrinsic phenotypic changes following genetic manipulations. Our approach reveals that known structural protein Lamin A/C is also a cell-cycle regulator and that known cell-cycle regulator cdk4/6 also affects nuclear and cell size.

Introduction

The cell cycle is a series of highly regulated steps that lead to controlled cell division. Typically, cells first prepare for DNA synthesis (G₁ phase), replicate their DNA (S phase), prepare for mitosis (G₂ phase), and undergo mitosis (M phase).^{1,2}

During this cell cycle, specific proteins serve as door guards at every phase to prevent cells from early entrance into the next stage of the cell cycle.³ Misregulation of the cell cycle in human and rodent cells has been implicated in a number of disease states.^{4–6} For example, mutated p53 causes cells to lose the function of the G₁/S checkpoint, replicating defective DNA, and finally leading to cancer.^{4,6} Flow cytometry (FC) is the instrument of predilection to measure cell-cycle distribution, particularly of adherent cells, and the effects of drug treatment or genetic alteration (knockdown, knockout, over-expression, *etc.*) on the cell cycle.^{7,8} A major advantage of FC is its ability to analyze a large number of cells in a short time. However, conventional FC analysis requires cells to be detached from their substrate and therefore cannot measure cell properties (*e.g.* nuclear shape, cell migration, cytoskeleton organization, *etc.*) at the same time in the same environment. Moreover, since the expression of a wide range of proteins greatly varies during the cell cycle,^{9–12} these cell properties may adopt significantly

^a Johns Hopkins Physical Sciences – Oncology Center, The Johns Hopkins University, Baltimore, Maryland 21218, USA. E-mail: wirtz@jhu.edu

^b Department of Chemical and Biomolecular Engineering, The Johns Hopkins University, Baltimore, Maryland 21218, USA

^c Department of Mechanical Engineering, The Johns Hopkins University, Baltimore, Maryland 21218, USA

^d Center for Strategic Scientific Initiatives, Office of the Director, National Cancer Institute, National Institute of Health, Bethesda, Maryland 20892, USA

^e Department of Ophthalmology, Washington University School of Medicine in St. Louis, St. Louis, Missouri, USA

† Electronic supplementary information (ESI) available. See DOI: 10.1039/c2ib20246h

‡ These authors contributed equally to this work.

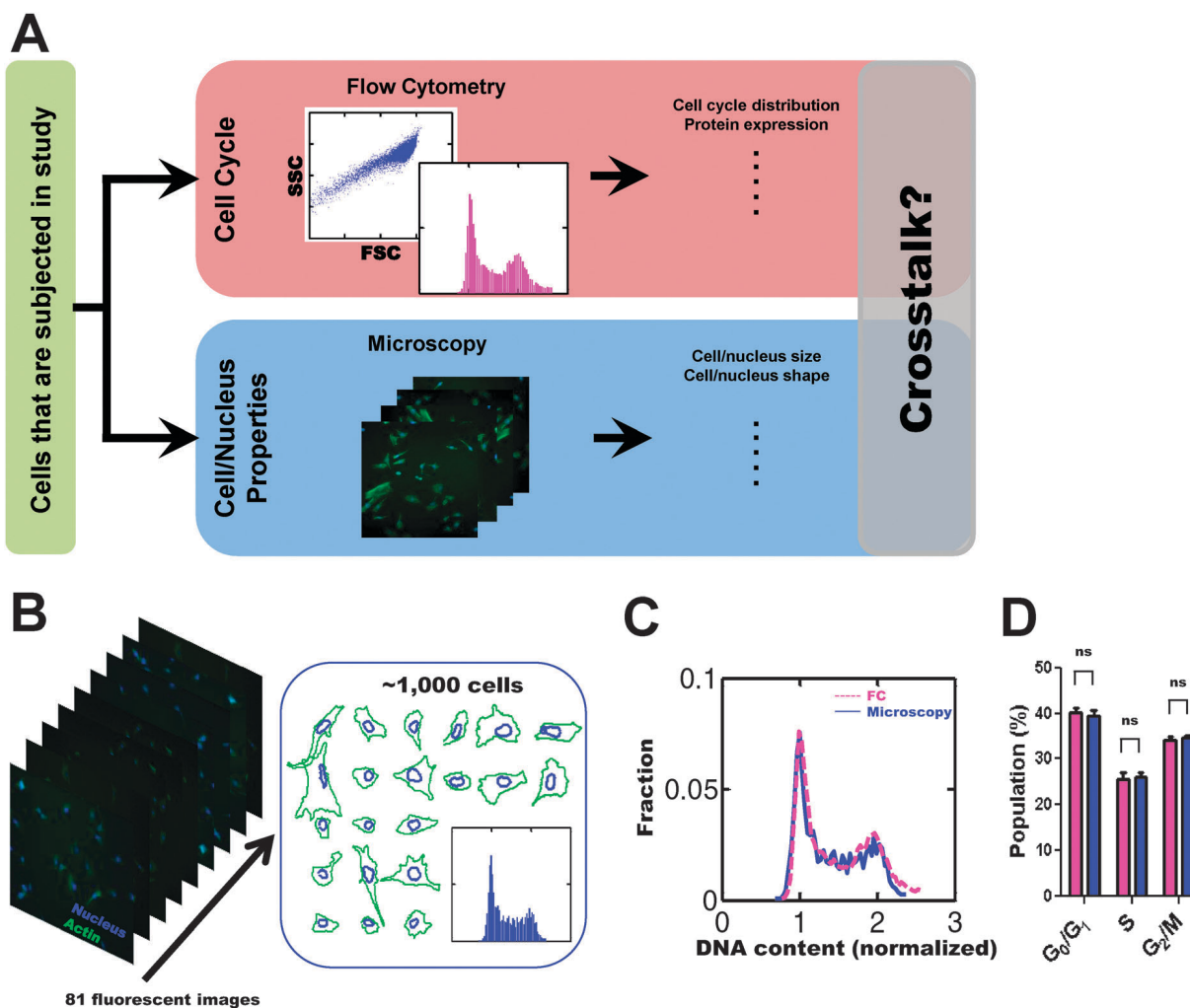


Fig. 1 Measurement of cell cycle phase distribution *in situ* – comparison with flow cytometry (FC). (A) Schematic showing that a common procedure to extract cell information is to run parallel experiments with different instruments. However, whether cell cycle and cell properties are linked, it still needs direct measurement to address. (B) Our microscopy-based high-throughput assay used in these studies to understand the question in panel A. Eighty-one fields of four-channel fluorescence/phase contrast images were automatically collected (only DNA channel in blue and actin channel in green are shown here) to analyze the intensity of ~ 1200 nuclei and simultaneously measure cell and nuclear properties (cell size, nuclear size, nuclear shape, etc.) in the same individual cells through edge detection of cell boundaries (green contours) and nuclear boundaries (blue contours). Inset: This analysis produced a DNA stain intensity distribution (blue profile). (C) Normalized DNA stain intensity distribution of c2c12 cells obtained from FC analysis (magenta profile) and our microscopy-based assay (blue profile). (D) Proportion of cells in the G_0/G_1 , S, and G_2/M cell-cycle phases, as measured by conventional FC analysis (magenta bars) and by microscopy-based analysis (blue bars). NS: non-significant differences; $p > 0.05$ (*t*-test for phase-to-phase comparison). Three biological repeats on different cells were conducted for both FC analysis and microscopy-based analysis.

different values in different phases. Consequently, without simultaneous measurement of cell cycle phases and cell properties in the same cells, an observed change in cell properties following a forced change in protein expression does not necessarily mean that this protein is a regulator of the cell property of interest. Rather this protein could be a cell cycle regulator (Fig. 1A).

Here we use a microscope-based assay to measure both the cell cycle phase of a thousand of individual adherent cells and their associated cellular and nuclear properties rapidly and simultaneously. This assay demonstrates that population-averaged cell morphological properties strongly depend on cell-cycle phases and could be written as linear combinations of cell-cycle fractions and phase-dependent morphological properties. This assay reveals that key structural nuclear-envelope

proteins (Nesprins, Lamin A/C) are regulators of nuclear size and nuclear shape partially because they affect cell cycle distribution; they are not *bona fide* (intrinsic) regulators of nuclear morphology.^{13–15} *Vice versa*, this assay indicates that inhibition of cell cycle regulators, cyclin-dependent kinase 4/6, cdk4/6, are also nuclear morphological regulators, and that some commonly used cell cycle synchronization methods have significant and lasting effects on cell and nuclear morphology.^{16,17}

Results and discussion

Measurements of cell cycle distributions *in situ*

First we established and validated a microscopy-based method to measure the cell-cycle phase in individual adherent cells. Mouse myoblasts (c2c12) were plated on a glass-bottom dish.

After 48 h incubation, cells were fixed, permeabilized, and incubated with nuclear DNA stain Hoechst 33342, a dye routinely used in FC analysis of cell cycle distribution,^{7,18} as well as additional stains to detect actin filament structures at the cell cortex and delineate the cytoplasm for cell edge detection (Fig. 1B). The dish was placed on a customized scanning fluorescence light microscope equipped with a motorized stage (Fig. 1B). Importantly, to quantitatively determine cell cycle phases at single-cell resolution, we introduced a calibration step to correlate measured Hoechst light intensity in the nucleus to the DNA content (see Methods). Light intensities from solutions of Hoechst molecules were measured using the same customized scanning microscope used subsequently to measure cell properties in the same cells (Fig. 1B). For each dish, reference illumination and dark images were collected and used to normalize the intensities in the illumination field (see additional details under *Methods*). This calibration step addressed potential non-uniform illumination of the samples by the light microscope and the non-uniform recording by the optical train of the microscope and the CCD camera.¹⁹

The cell cycle-phase distribution of c2c12 mouse myoblasts measured by this microscopy-based assay was carefully compared to the cycle-phase distribution obtained from conventional FC analysis (Fig. 1C and D).⁷ For both methods, cells were fixed and their DNA was stained with the same nuclear DNA dye Hoechst 33342. Even though different numbers of cells were assessed (~10 000 cells for FC vs. 1000–2000 for our assay), cell cycle distributions were statistically indistinguishable (Fig. 1C and D). By zooming in on the G₀/G₁ phase peak, we found that the coefficients of variation (CV) of these cell sub-populations using Gaussian fits were close, and that the signal-to-noise ratios (1/CV) were highly similar (Fig. 1D and Table 1).²⁰

A direct comparison between FC analysis and the analysis provided by our assay also showed statistically indistinguishable cell cycle distributions for human breast carcinoma cells (MD-MB-231) (Fig. S1, ESI[†]). Our assay was not limited to c2c12 and MD-MB-231 cell lines. We tested seven additional types of adherent cells and found that our assay could readily measure

their cell-cycle distributions (Fig. S2, ESI[†]). These cells were chosen to determine whether our assay worked on both normal and disease cells, immortalized and primary cells, as well as human and rodent cells. The tested cells include human pancreatic normal epithelial cells, patient-derived pancreatic cancer ductal adenocarcinoma cells harvested from the primary tumor and from liver metastatic sites, normal human breast epithelial cells (MCF10A), and primary mouse embryonic fibroblasts (Fig. S2, ESI[†]).

Simultaneous measurements of cell cycle and cell and nuclear morphology in adherent cells

Next, we used the same microscopy method to measure both cell-cycle phases and cell and nuclear properties simultaneously in the same adherent cells. Flow cytometry can simultaneously measure cell size and the DNA content in suspension cells. However, other important morphological properties of adherent cells including cell shape and nuclear shape become effectively meaningless if adherent cells are (artificially) detached from their substrate. Moreover, spatial information is lost. We measured the DNA content of cells in culture and color-coded nuclei according to the associated cell cycle phase (Fig. 2A and B). In the same cells, we measured nuclear size and shape and cellular size and shape to determine not only population-averaged values of these properties, but also their phase-dependent values (Fig. 2C–F). As would be expected, cell and nuclear size increased as cell cycled from the G₀/G₁, S, and G₂/M phases (Fig. 2D, F, H, and J). More unexpectedly, we found that nuclei became more elongated during cycle progression, information lost using conventional approaches. Together these results show that our microscopy assay can measure the following six independent quantities simultaneously: the three percentages of cells in each phase of the cell cycle (f_{G_0/G_1} , f_S , and $f_{G_2/M}$; Fig. 1 and 2B) and the three associated values of the cell property x (e.g., cell shape, nuclear shape, etc.) in each phase, x_{G_0/G_1} , x_S , and $x_{G_2/M}$, which are typically different from each other.

Cell properties depend critically on cell cycle phase

To help clarify the potential influence of cell cycle-phase distribution on cell properties (such as nuclear size or cell shape),²¹ we wrote the mean value of a given cell property $\langle x \rangle$ as a linear combination of cell fractions in each phase and mean values of the cell property in each of the cell cycle phase:

$$\begin{aligned} f\langle x \rangle &= f_{G_0/G_1}x_{G_0/G_1} + f_Sx_S + f_{G_2/M}x_{G_2/M} \\ &= \sum_{i=G_0/G_1}^{G_2/M} f_i x_i \end{aligned} \quad (1)$$

Here, $\langle x \rangle$ is the cell population-averaged value of the cell property being considered (e.g. the cell population-averaged values of nuclear and cell sizes and shapes), x_i are the mean values of this property in the cell-cycle phases i ($i = G_0/G_1, S,$ and G_2/M phases), and f_i are the fractions of cells in each phase i , which is also the relative time that cells spend in each phase of

Table 1 Resolution of cell cycle phase determination: FC vs. microscopy-based assay

	Population in G ₀ /G ₁ (%)	Population in S (%)	Population in G ₂ /M (%)	SNR	R ₂
FC	40.3	25.6	34.1	8.6	0.97
FC (sampled)	39.4	28.5	32.1	9.1	0.88
Microscopy	39.3	26.1	34.6	8.3	0.92

Fractions of cells in each cell cycle phase estimated by FC analysis and the microscopy-based assay showed no statistical difference (Fig. 1). The resolution of the cell cycle-phase distributions obtained by these two methods was estimated by Gaussian fits of the G₀/G₁ peaks. The coefficient of variation (CV) is defined as the ratio of standard deviation over mean value. Signal to noise ratio (SNR) is the reciprocal of the coefficient of variation. Cells in the G₀/G₁ phase were analyzed by: (i) flow cytometry (denoted FC) using 10 000 cells, (ii) flow cytometry using the same number of cells as analyzed by our microscopy-based assay (1000 cells; denoted FC (sampled)), and (iii) by our microscopy-based assay.

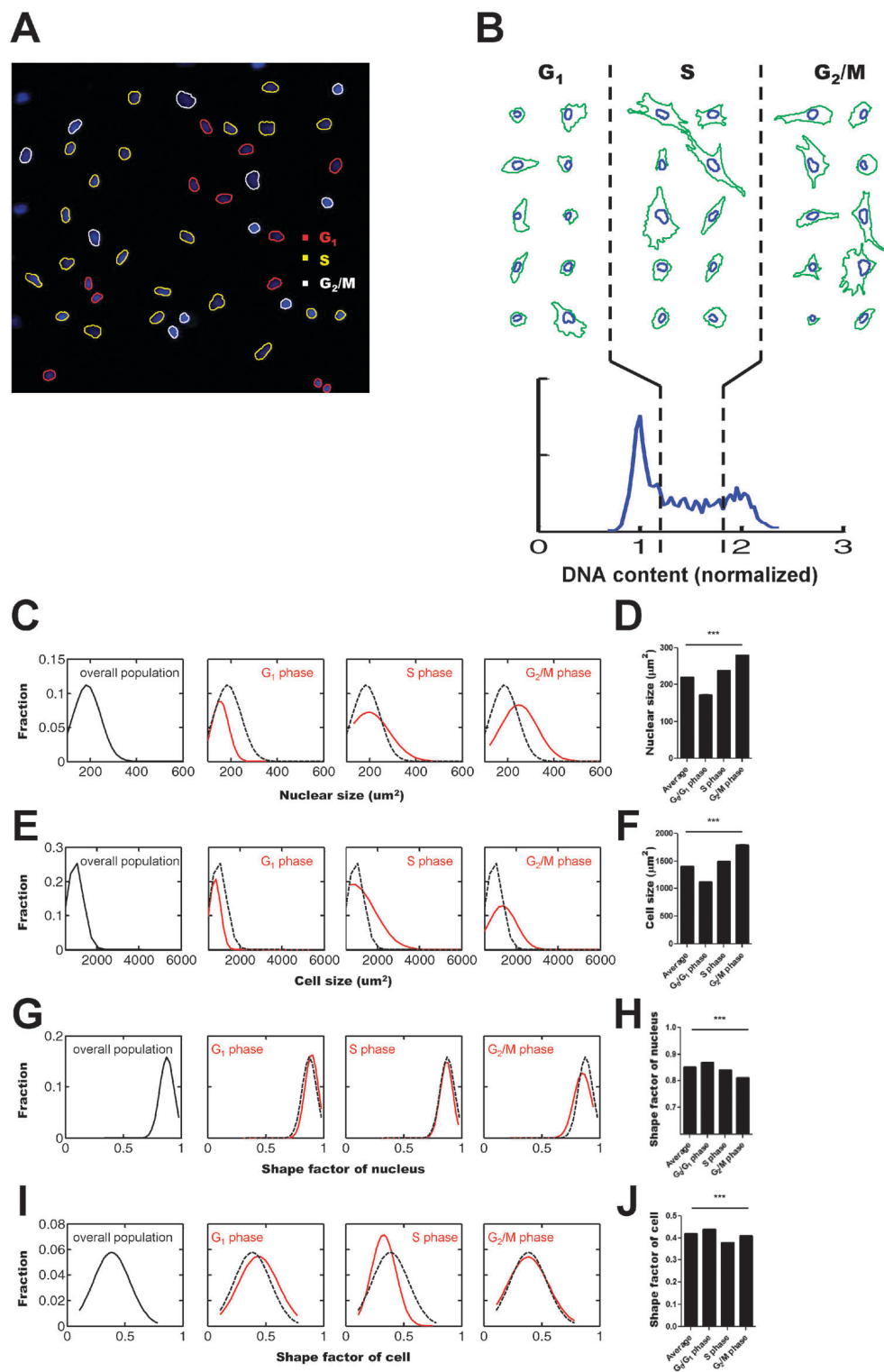


Fig. 2 Simultaneous measurements of cell cycle phase and cell properties in adherent cells. (A) c2c12 mouse myoblasts in culture were stained with DNA and F-actin stains and DNA content was quantified following a calibration step (see Methods section); nuclei were color-coded according to their cell cycle phase. This illustrates how the position of cells in the culture dish is not lost, unlike for FC for which cells are detached before cell-cycle and phenotypic assessments. (B) For the sake of clarity, c2c12 cells were computationally placed on a grid, depending on their cell-cycle phase. This illustrates how DNA content distribution is measured using direct measurement of DNA stain intensity in adherent cells. Cells contours are in green, nuclear contours are in blue. (C–H) Distributions and averaged values of nuclear size (C and D), cell size (E and F), nuclear size (G and H) and nuclear shape (I and J) measured by our assay. Population-based distributions of cell and nuclear properties, for which no distinction among phases is made, are shown in black. Distributions of cell and nuclear properties for the G_0/G_1 phase, the S phase, and the G_2/M phase are shown in red (panels C, E, G). In panel D, F, H, J, all apparent differences are statistically significant, $p < 0.0001$ (one-way ANOVA) as compared to population-averaged values of the considered phenotype. Three biological repeats conducted on different cells were analyzed for a total of >3000 cells for each tested condition.

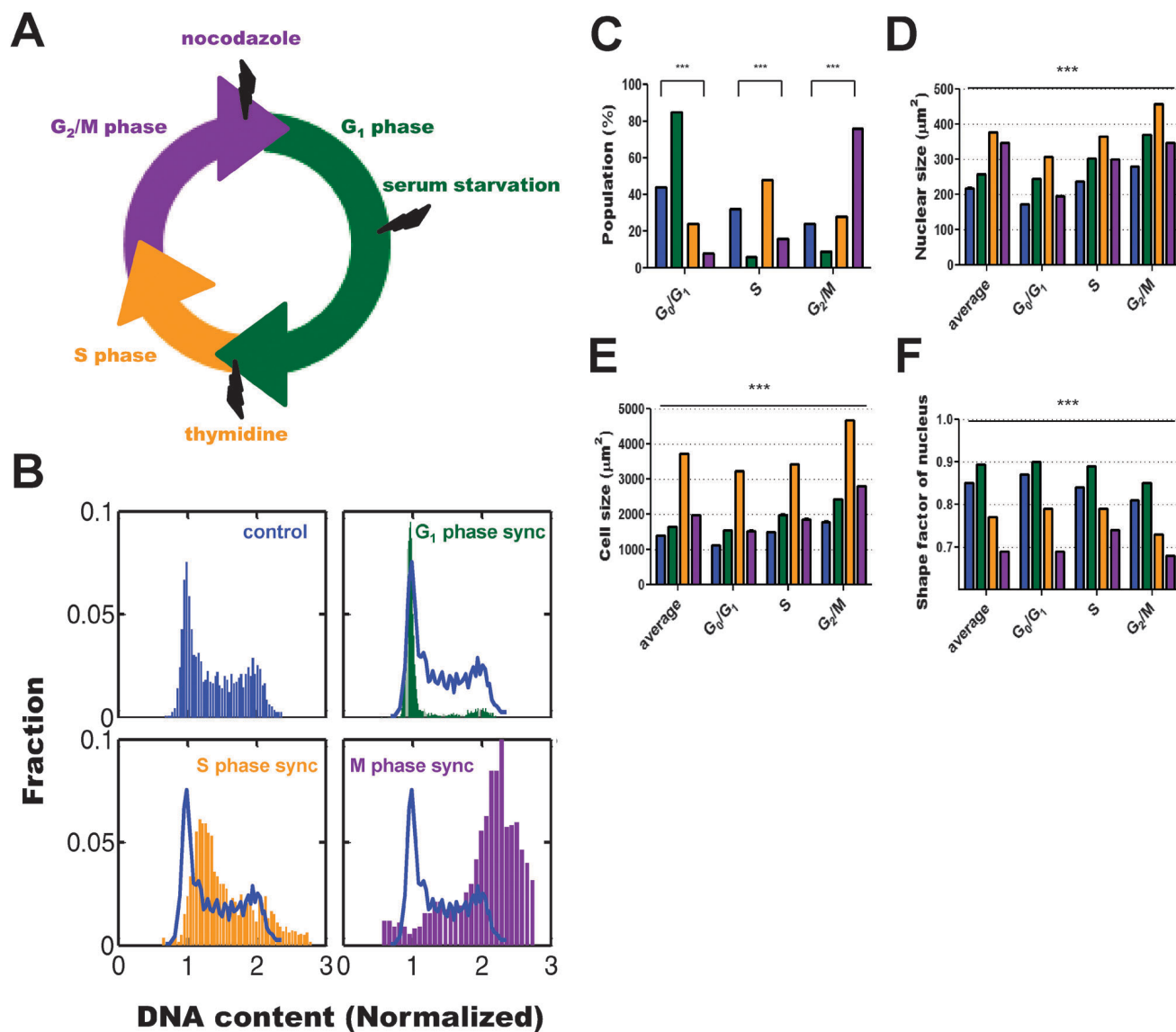


Fig. 3 Conventional cell cycle synchronization methods cannot be used to measure cell-cycle-dependent nuclear/cellular properties. (A) Ubiquitously used methods were applied to synchronize the phase of c2c12 cells. These include serum-starvation which enriches cells in the G₁ phase (green), nocodazole treatment which enriches cells in the M phase (purple), and thymidine treatment which enriches cells in the early S phase (orange). (B) Cell-cycle phase distributions obtained by microscopy-based analysis of untreated control asynchronous cells (blue bars), and serum-starved cells (green bars), thymidine-treated cells (orange), and nocodazole-treated cells (purple). The contour of the cell-cycle distribution for control cells (blue) is shown in each case to help visual comparison. (C) Proportion of cells in the G₀/G₁, S, and G₂/M phases for control (blue bars), serum-starved (green), thymidine-treated (orange bars), and nocodazole-treated cells (purple bars). (D-F) Population-averaged values and cell-cycle-phase-dependent mean values of nuclear size (D), cell size (E), and nuclear shape (F), compared phase-to-phase, induced in serum-starved (green), thymidine-treated (orange), and nocodazole-treated cells (purple) in each phase compared to control cells (blue). All apparent differences are statistically significant, $p < 0.0001$ (one-way ANOVA) as compared to phenotypic values for control cells in each corresponding phase. For panels B–F, three biological repeats conducted on different cells were analyzed for a total of >3000 cells for each tested condition.

the cell cycle. The method presented here enables us to measure x_i and f_i separately and simultaneously in the same cells.

When assessing the role of the expression or activity of a protein in a given cell function, cells are typically subjected to a drug that specifically inhibits/activates the protein or the gene of interest is knocked down (KD), knocked out (KO) or over-expressed. It is then pervasively assumed that any measured change in mean cell property (*i.e.* a change in the population averaged value $\langle x \rangle$) reflects the involvement of this protein in the cell function being assessed, without considering the

possible redistribution of the cells along the cell cycle. For example, the nuclear lamina-associated structural proteins, Nesprins, are widely believed to be structural regulators of nuclear shape because of their role in physically connecting the nuclear lamina to the cytoskeleton and because the depletion of Nesprins changes nuclear roundness.^{13,22–24}

This approach to assess the role of a protein in cell functions is only legitimate if the fractions f_i of cells in the different cell-cycle phases remain unchanged following application of the inhibitor/activator or genetic manipulation, *i.e.* that the

protein of interest is not also a cell cycle regulator. Alternatively, when in doubt that it is actually correct and that cell properties could be cell-cycle dependent, then cells can be synchronized. To synchronize cells, cells are often subjected to serum-starvation or chemicals that arrest cells in a specific phase of the cell cycle (Fig. 3A).^{8,25–27} While used routinely in cell biology, such chemical treatments can induce their own side effects, including the fact that they may not synchronize cells. For instance, thymidine arrests cells in the early S phase. However, thymidine treatment to assess cell phenotypes in the S phase is only correct if the cell properties, x_i , are the same for S-phase-synchronized cells as the cell properties of non-synchronized cells that are happen to be in the S phase. The same assumption is typically made when cell synchronization is induced by serum starvation or cell treatment with the microtubule depolymerizing drug nocodazole, which enriches the G_0/G_1 phase and M phase, respectively.

Exploiting the advantage that our assay can measure cycle phases and cell properties in the same individual cells simultaneously, we tested whether these commonly used cell synchronization methods verified this assumption. Surprisingly, synchronization methods, such as serum starvation and thymidine/nocodazole treatments, affected not only cell cycle distributions, as expected, but also greatly changed cell and nuclear properties (Fig. 3B–F). Results from our analysis confirmed that, as expected, these methods of synchronization did enrich cells in the target cycle phase: the S phase for thymidine treatment (orange), the G_1 phase following serum starvation (green), and the M phase for nocodazole treatment (purple, Fig. 3B and C). However, these synchronization methods also had a significant and lasting effect on cell properties in every cell cycle phase (Fig. 3D–F). For instance, thymidine treatment greatly increased the size of cells in the enriched S phase by 120% compared to untreated cells in the same S phase, *i.e.* the mean size of treated cells in the S phase was 2.2 times the mean size of untreated cells in the S phase. The mean size of thymidine-treated cells in the enriched G_0/G_1 and G_2/M phases was similarly increased by 130% and 220% compared to untreated (asynchronous) cells in the same G_0/G_1 and G_2/M phases, respectively. Serum starvation and nocodazole treatment fared somewhat better, but still changed measured cell properties by >30%, including a 75% increase in cell size for nocodazole-treated cells in the G_2/M phase. If synchronization were non-invasive, these phenotypic changes should have been vanishingly small.

More importantly, we verified that adding back serum to serum-starved cells or washing cells to eliminate the synchronizing drug from the medium allowed cells to recover the cycle-phase distribution of untreated cells prior to forced synchronization within 24 h (Fig. S3A and B, ESI†). However, changes in cell and nuclear properties did not recover their untreated values, *i.e.* all tested synchronization methods continued to affect cell/nuclear size and cell/nuclear shape, even 24 h after release (Fig. S3C and D, ESI†). Together these results indicate that commonly used synchronization methods are not appropriate to reduce or eliminate possible effects of

cell cycle re-distribution on cell properties, as they do not keep cell properties constant in the enriched phase compared to the value of the property in untreated cells in that phase. One should use synchronization methods with caution, and should not ignore the effect of changes in phenotypic property associated with forced synchronization.

The role of cell cycle regulator in cell phenotype regulation

Next, we asked whether inhibition of well-characterized cell cycle regulators, such as Cdk4/6, could also inadvertently affect cellular phenotypes. Eqn (1) suggests that a change in the cell-population-averaged value of the cell phenotype (\bar{x}) (say nuclear size) following protein inhibition could result from cell-cycle redistribution (*i.e.* changes in f_i). As expected, treatment of cells with specific Cdk4/6 inhibitor IV, *trans*-4-((6-(ethylamino)-2-((1-(phenylmethyl)-1*H*-indol-5-yl)amino)-4-pyrimidinyl)amino)-cyclohexanol (CINK4), blocked cells in the G_0/G_1 phase and reduced the population of cells in the S and G_2/M phases (Fig. 4A).²⁸ Moreover, Cdk4/6 inhibition also significantly affected population-averaged nuclear and cell morphology (*e.g.* ~50% decrease in nuclear size accompanied by rounding of the nucleus) (Fig. 4B–D), and continued to affect cell properties up to 6 h after release (Fig. S3E and F, ESI†). However, our assay which can evaluate cell-cycle-dependent values of phenotypes simultaneously (*i.e.* changes in x_i) revealed that inhibition of Cdk4/6 caused significant effects on the values of phenotypes in each phase. For instance, following Cdk4/6 inhibition, the nuclear size of cells in the G_0/G_1 phase decreased by >50% ($p < 0.0001$). Hence our assay suggests that besides its well-known

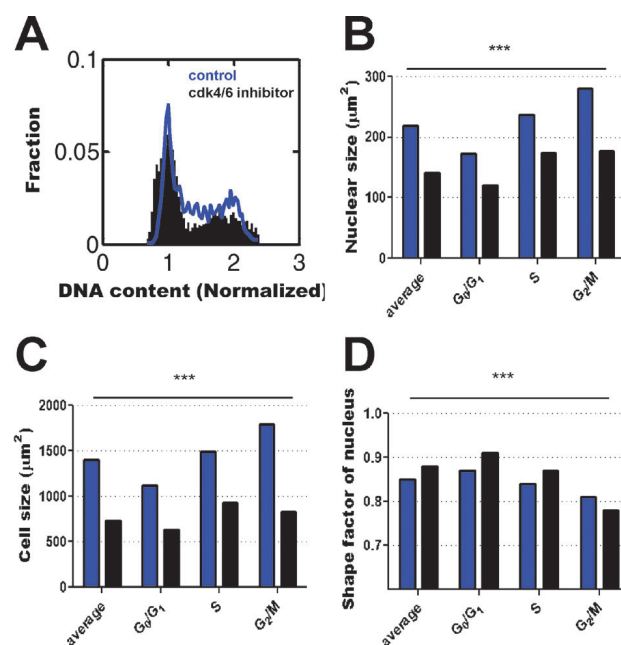


Fig. 4 Inhibition of cell cycle regulator, cdk4/6, causes changes in cell properties. (A) Cell-cycle distributions of control cells and cells treated with Cdk4/6 inhibitor IV. Blue represents control. Black represents Cdk4/6 inhibitor IV treatment. (B–D) Population-averaged (first bars) and cell-cycle-dependent nuclear size (B), cell size (C), and nuclear shape factor (D). Three biological repeats on different cells were analyzed for a total of >3000 cells for each tested condition.

central role in cell cycle, Cdk4/6 may also play a structural role by regulating nuclear morphology.

The role of structural proteins in cell cycle regulation

Having manipulated cell cycle distributions through various forced synchronization schemes or Cdk4/6 inhibition to determine their (unexpected) effect on cellular and nuclear properties in each phase, we next manipulated cell properties through shRNA-mediated depletion of seemingly well-established structural regulators of these properties, while simultaneously measuring potential changes in cell cycle distribution. To help clarify this test, we return to eqn (1). For a protein to be an “intrinsic” regulator of cell/nuclear morphology, that protein should not have the side effect of significantly affecting cell cycle distribution (which in turn would affect cell properties, Fig. 1A): the depletion of that protein should mostly induce changes in cell properties x_i , not changes in cell cycle fractions f_i .

Nuclear lamina protein Lamin A/C, which forms a thin elastic filamentous meshwork underneath the nuclear envelope and penetrates the intranuclear space, and LINC complex molecules Nesprin2giant and Nesprin3, which physically connect the nuclear lamina to the cytoskeleton, have recently been established as major structural proteins that regulate nuclear size and nuclear shape.^{29–32} Indeed, we found that shRNA-mediated depletion of Lamin A/C, Nesprin2giant and Nesprin3

all significantly deformed and decreased the size of the nucleus and cell in all phases of the cell cycle (“average bars” in Fig. 5C–E).

However, the depletion of these nuclear envelope proteins also affected cycle-phase distribution (Fig. 5A and B).^{14,33,34} For instance, shRNA-mediated depletion of Lamin A/C significantly enriched the G_0/G_1 phase, while reducing the fractions of cells in the S and G_2/M phases (Fig. 4B). This result was confirmed in primary $LMNA^{+/+}$ and $LMNA^{-/-}$ mouse embryonic fibroblasts (Fig. S4, ESI[†]): Lamin A/C deficiency enriched the G_0/G_1 phase, while reducing the number of cells in other phases. Depletion of Nesprin3 also significantly enriched the G_0/G_1 phase and slightly, but significantly, reduced the fractions of cells in the S and G_2/M phases. Nesprin 3 depletion had a much larger effect on cell cycle redistribution than Nesprin2giant (Fig. 5B).

Our assay allowed us to assess changes in nuclear size, phase by phase (for example, by comparing the mean values of nuclear size in the G_2/M phase of both control cells and shRNA-depleted cells directly) (Fig. 5D–I). Furthermore, the assay revealed that the role of Lamin A/C and Nesprins in nuclear morphology and cell size strongly depended on cell-cycle phases (Fig. 5C–E). For instance, depletion of Lamin A/C and Nesprins had a 3-fold greater effect on nuclear size for cells in the G_0/G_1 phase than cells in the G_2/M phase (Fig. 5C). Together these results showed that while Lamin A/C,

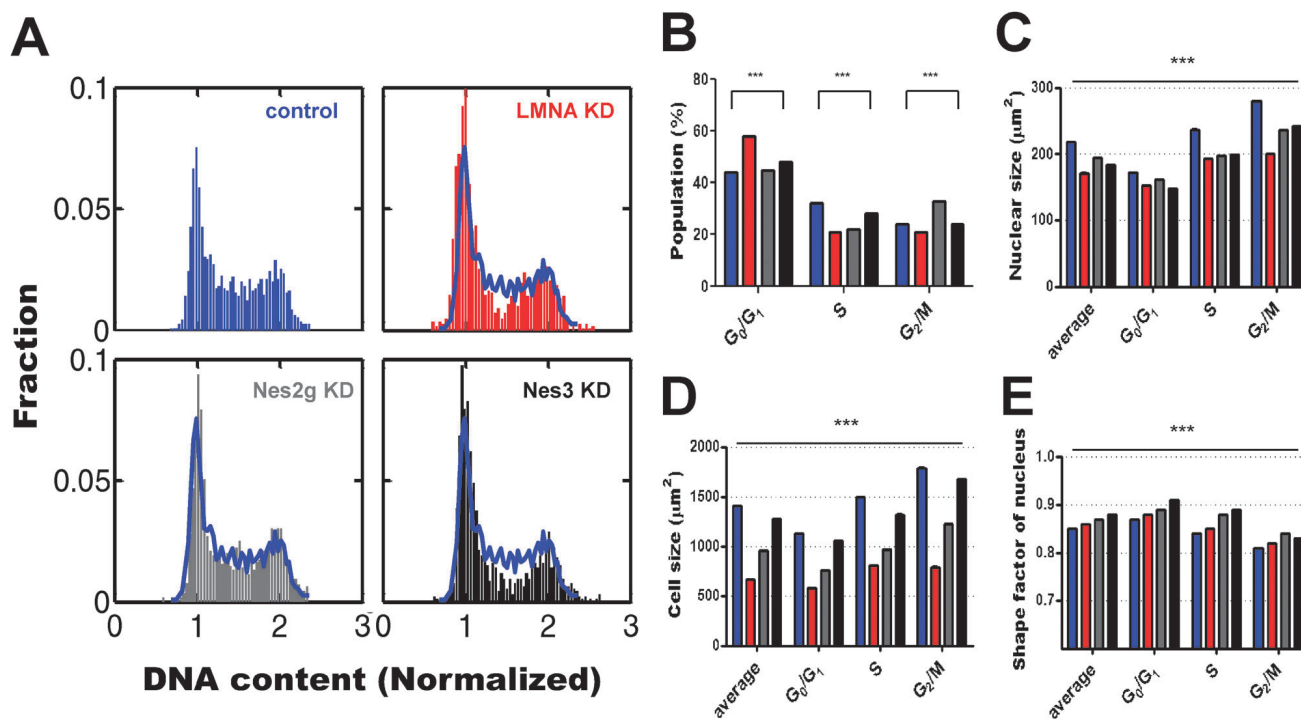


Fig. 5 Combined measurements of cell cycle phase and cell properties reveal *bona fide* regulators of cell phenotypes and cycle phase. (A) Cell cycle distributions obtained by microscopy-based analysis of control cells (blue) and cells depleted of nuclear envelope-associated proteins Lamin A/C (red), Nesprin3 (black), or Nesprin2giant (grey). The profile of the cell cycle distribution for control cells (blue) is shown for visual comparison. (B) Proportions of cells in the G_0/G_1 , S, and G_2/M phases for control (blue bars), Lamin A/C-depleted cells (red), Nesprin3-depleted cells (black), and Nesprin2giant-depleted cells (grey) (B). (C–E) Cell-cycle-phase-dependent mean values of nuclear size (C), cell size (D), and nuclear shape (E), compared phase to phase, induced in each phase by depletion of Lamin A/C (red), depletion of Nesprin3 (grey), and depletion of Nesprin2giant (black) compared to control cells (blue). All apparent differences are statistically significant, $p < 0.0001$ (one-way ANOVA) as compared to phenotypic values for control cells in each corresponding phase. Three biological replicates were analyzed for all tested conditions (panels A–E).

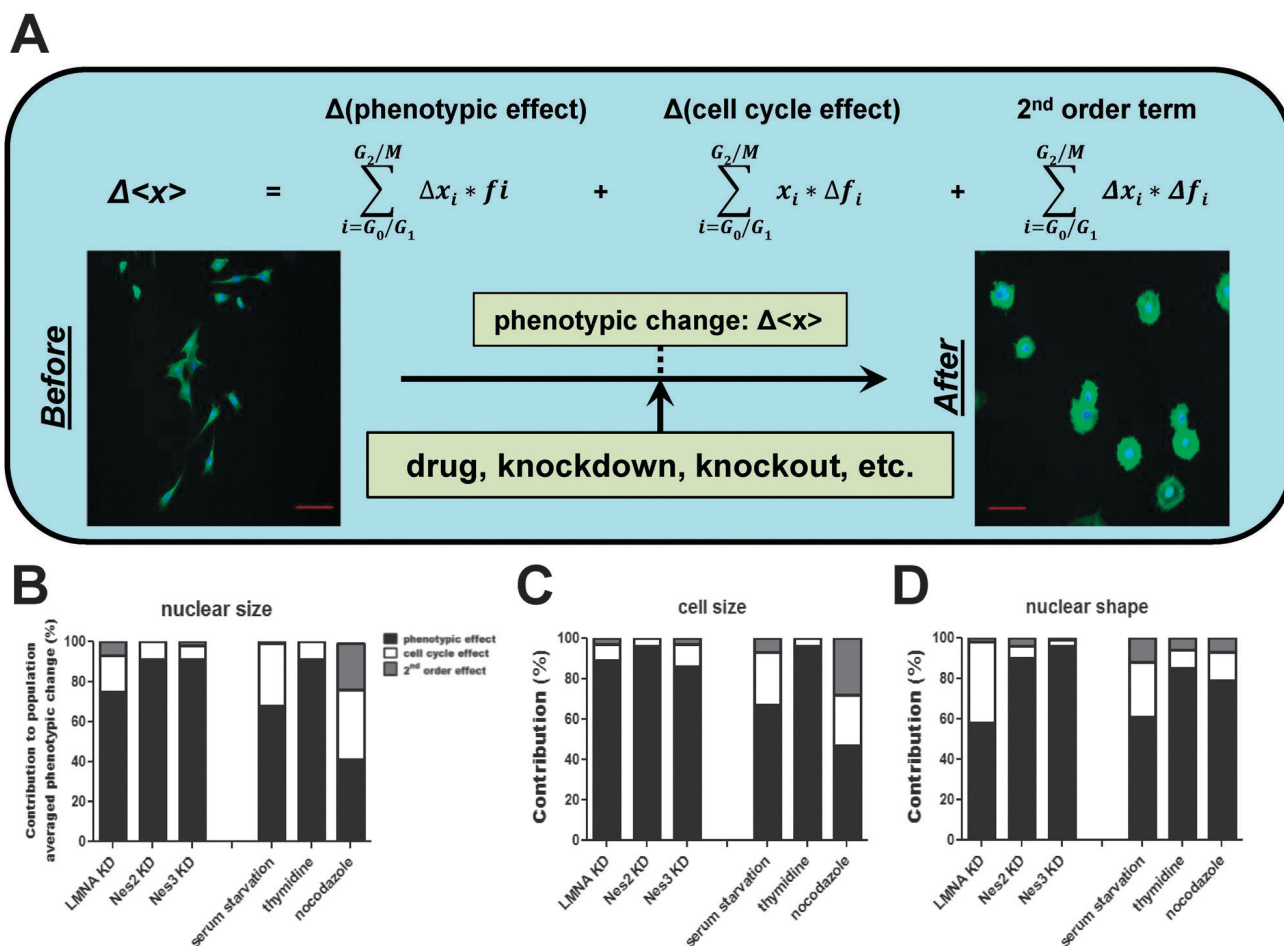


Fig. 6 Contribution of cell cycle redistribution to population-averaged changes in cell properties. (A) Changes in the population-averaged values of cell/nuclear properties can be expressed as a sum of three major contributions: $\Delta x = \langle x \rangle_{\text{control}} - \langle x \rangle_{\text{KD or Drug}} = \sum_{i=G_0/G_1}^{G_2/M} \Delta x_i f_i |_{\text{control}} + \sum_i \Delta f_i x_i |_{\text{control}} + \sum_i \Delta f_i \Delta x_i$. Here Δx_i is the total change in the population-averaged value of the cell/nucleus property of interest caused by the depletion (denoted by lowercase KD) of either Nesprin2giant, Nesprin3, or Lamin A/C or induced by forced synchronization (lowercase Drug) compared to control cells; Δx_i are the same differences but evaluated for cells in each cell-cycle phase i ; and Δf_i are the changes in cell-cycle fractions for each phase i . The summation Overall changes in cell properties, Δx , may stem from three distinct contributions: changes in intrinsic cell properties independent of changes in cell cycle (first term), indirect changes in cell properties due a change in cell cycle distribution (second term), and coupled changes in cell cycle and cell properties (third term), which are expected to be second-order in magnitude. (B–D) Contributions to global changes in population-averaged nuclear size (B), cell size (C) and nuclear shape (D) due to intrinsic cell-cycle-independent changes in these properties (black), due to cell cycle redistribution (white), and due to coupled effects of cell cycle redistribution and intrinsic cell-cycle-independent changes in nuclear size (grey). This analysis was applied to c2c12 cells depleted of Lamin A/C, cells depleted of Nesprin2giant, and cells depleted of Nesprin3, as well as c2c12 cells subjected to serum-starvation, cells treated with thymidine, and cells treated with nocodazole. Three biological replicates were analyzed for all tested conditions (panels B–D).

Nesprin2giant and Nesprin3 should be considered both regulators of nuclear morphology and cell cycle phase distribution, which indirectly affect nuclear morphology.

Distinct contributions to global changes in cell properties from cell-cycle redistribution vs. intrinsic changes in cell properties

When cells are subjected to nocodazole or thymidine treatments, serum starvation, or shRNA-depletion of structural proteins such as Lamin A/C and Nesprins, the population-averaged mean values of nuclear size, cell size, and nuclear shape change (Fig. 3 and 5). We can quantify the contributions to changes in these mean values due to: (i) direct changes in intrinsic values of these properties (“phenotypic effect”, Fig. 6A), *i.e.* changes in the cell-cycle-independent values of these properties, (ii) indirect changes due to cell cycle

re-distribution (“cell cycle effect”, Fig. 6A), and (iii) second-order effects due to coupled phenotypic changes and cell cycle distribution (“2nd order term”, Fig. 6A). Indeed, one can easily show that the global change in a cell property x can be written as:

$$\begin{aligned} \Delta x &= \langle x \rangle_{\text{control}} - \langle x \rangle_{\text{KD or Drug}} \\ &= \sum_{i=G_0/G_1}^{G_2/M} \Delta x_i f_i |_{\text{control}} + \sum_i \Delta f_i x_i |_{\text{control}} + \sum_i \Delta f_i \Delta x_i \end{aligned} \quad (2)$$

Here Δx is the total change in the mean value of nuclear size, cell size, and nuclear shape caused by shRNA-mediated depletion (subscript KD) of Nesprin2giant, Nesprin3, or Lamin A/C or by pharmacological synchronization or protein inhibition (subscript Drug) compared to control cells; Δx_i are the same

differences but evaluated for cells in each cell-cycle phase i ; and Δf_i are the changes in cell-cycle fractions for each phase i . Therefore, overall changes in cell properties following protein depletion or drug treatment may stem from three distinct contributions: (i) intrinsic changes in cell properties independent of changes in cell cycle-phase distribution (first term in eqn (2)), indirect changes in cell properties due a cell cycle-phase redistribution (second term), and coupled changes in cell cycle and cell properties (third term), which are expected to be second-order in magnitude (Fig. 6A). For cells depleted of structural proteins such as nuclear-envelope-associated Nesprins, changes in cell properties should mostly be due to the first term, which means that $\Delta f_i \approx 0$ in eqn (2) and, in turn, $\Delta x \approx \sum \Delta x_i f_{i\text{control}}$. For cells subjected to synchronization by serum-starvation or drug treatment, changes in cell properties should mostly be due to the second term (*i.e.* due to cell-cycle redistribution), which means that $\Delta x_i \approx 0$ in eqn (2) and $\Delta x \approx \sum \Delta x_i f_{i\text{control}}$. Here $f_{i\text{control}}$ and $x_{i\text{control}}$ are the fractions of cells and values of the cell property of interest in phases i for control cells.

Here, we found that overall changes in nuclear size upon depletion of Lamin A/C due to direct intrinsic changes in nucleus size (when properly compared phase-to-phase) was only 75%, and that the contribution due to cell-cycle redistribution was significant (>20%) (Fig. 6B). Depletion of Nesprin2giant and Nesprin3 still induced 9% contribution to global change in nuclear size from cell cycle re-distribution (Fig. 6B). Similar conclusions held for changes in cell size (Fig. 6C) and nuclear shape (Fig. 6D): changes in cell size and nuclear shape by depletion of Lamin A/C, Nesprin3, or Nesprin2giant were partly due to non-negligible contributions from cell cycle re-distribution.

Vice versa, we analyzed the contributions of (unwelcome) changes in cell/nuclear properties following forced synchronization by serum starvation, thymidine treatment, or nocodazole treatment (Fig. 6B–D). Ideally, if synchronization was non-invasive, then the contribution from the first term in eqn (2) to changes in nuclear shape and size would be 100% and the contribution from the other terms would be zero. Remarkably, we found that the contributions to changes in nuclear size due to forced cell-cycle redistribution were significantly smaller than the contributions from intrinsic changes in nuclear size: only 31% for serum starvation, 9% for thymidine treatment, and 35% for nocodazole treatment were due to changes in nuclear size induced by forced synchronization compared to contributions of 68%, 91%, and 41% that were due to (uncontrolled) changes in nuclear size in each phase (Fig. 6B). Similar conclusions held when assessing changes in nuclear size and nuclear shape (Fig. 6C and D).

A literature survey indicates that the vast majority of biological studies that make use of shRNA-induced depletion or genetic knockout or over-expression of specific proteins as methods to assess the function of a protein in mammalian cells only use changes in population-averaged values of the cell property under study (the left hand-side of eqn (2)) as a way to quantitatively assess a protein function in cell physiology,

without taking into account possible changes in phase distribution caused by these cell manipulations. The remainder of these studies used forced synchronization as a way to reduce cell-cycle-dependent effects, and none measured both changes in cell properties and cell cycle distribution at the same time, as presented in this study. Our results suggest that this general approach to assess the role of proteins in establishing cell and nuclear properties could lead to erroneous conclusions.

Here, we used a microscopy-based assay that allowed us to measure cell cycle phases and cell/nuclear properties simultaneously in the same cells. This assay: (i) distinguished *bona fide* cell-cycle-independent regulators of cell and nuclear properties from cell-cycle-dependent regulators that regulate cell properties only or partially though cell cycle redistribution, (ii) revealed new regulators of cell cycle distribution (*e.g.* Nesprin2giant and Nesprin3 were not known to be cell cycle regulators), and (iii) quantified the distinct contributions of specific proteins to cell properties due to direct/intrinsic regulation by these proteins and due to indirect changes caused by uncontrolled cell cycle redistribution.

This study illuminates the critical importance of measuring cell and nuclear properties in each cell phase, highlights and quantifies the danger of using commonly used synchronization methods to eliminate potential effects of cell cycle redistribution on cell phenotypes, and suggests that regulators of other cell functions (*e.g.* nuclear morphology, cell motility), previously identified through shRNA-mediated depletion or knockout studies, may indeed be mixed cell-property/cell-cycle regulators.

Methods

Cell culture, cell synchronization, and pharmacological treatments

Mouse myoblasts (c2c12) were cultured in Dulbecco's Modification of Eagle's Medium (DMEM) (Invitrogen, Carlsbad, CA) supplemented with 10% of fetal bovine serum (FBS, Hyclone, Logan, UT) and 100 U penicillin and 100 μg streptomycin (Sigma, St. Louis, MO) and 0.1% of puromycin. Human breast cancer cells, MDA-MB-231 (ATCC, Manassas, VA), and freshly harvested *LMNA*^{+/+} and *LMNA*^{-/-} mouse embryonic fibroblasts were cultured in DMEM with 10% of FBS and 100 U penicillin and 100 μg streptomycin. Human transformed epithelial cells, MCF-10A, were cultured in DMEM F-12 medium (Invitrogen) with 5% of horse serum, 0.5 $\mu\text{g ml}^{-1}$ of hydrocortisone, 20 ng ml^{-1} of hEGF, 10 $\mu\text{g ml}^{-1}$ of bovine insulin (Sigma), and 100 $\mu\text{g ml}^{-1}$ cholera toxin (Sigma). Human pancreatic normal epithelial cells (HPNE) were cultured in DMEM (low glucose), M3 base medium, FBS, Gentamicin, EGF, P/S (Sigma). Patient-derived pancreatic ductal adenocarcinomas, liver metastasis and primary tumor cells were cultured in DMEM with 10% of FBS and 100 U penicillin and 100 μg streptomycin. The culture environment was maintained at 37 °C and 5% CO₂. Cells were passaged every three days.

For each type of cell, ~10 000 cells were plated on a glass bottom dish (World Precision Instruments, Sarasota, FL). After incubation for 48 h, the treatment for synchronization was applied.

To serum-starve cells, cells were washed three times with Hanks' balanced salt solution (HBSS) (GBICO) and cultured in serum-free medium for 72 h. For synchronization at early S phase, cells were treated with 2 mM of thymidine for 18 h twice. Between these two treatments, cells were rinsed with HBSS three times and cultured in normal growth medium to release the cell cycle for 9 h. To synchronize cells in the M phase, cells were first treated with 2 mM of thymidine for 24 h. Followed by rinsing with HBSS three times, cells were released with normal growth medium for 3 h. After the short release, cells were treated with 100 ng ml⁻¹ of microtubule-depolymerizing drug nocodazole for 12 h. For inhibition of Cdk4/6, cells were treated with 10 nM *trans*-4-((6-(ethylamino)-2-((1-(phenylmethyl)-1*H*-indol-5-yl)amino)-4-pyrimidinyl)amino)-cyclohexanol (CINK4) Cdk4/6 inhibitor (EMD Chemical) for 24 h, prior to cell cycle and phenotypic analysis.

Flow cytometry

Our protocol follows that from Current Protocol from Cytometry (Wiley).¹⁸ Briefly, cells were grown in a 10 cm dish for 48 h, then trypsinized, spin down at 1000 rpm for 5 min, and resuspended in fresh culture medium without any serum. 10⁶ cells per ml were resuspended with a final concentration 5 µg ml⁻¹ of Hoechst 33 342 and incubated for 30 min at room temperature. After incubation, cells were spin down to remove the dye solution, resuspended in fresh culture medium, and then promptly subjected to flow cytometry. The raw data were extracted with FlowJo software (Tree Star Inc., Ashland, OR) and processed with Matlab.

High-throughput fluorescence microscopy

Cells were fixed with 3.7% of formaldehyde (Sigma) for 15 min at room temperature (RT). After fixation, cells were permeabilized with 0.1% Triton X-100 (Sigma) for 10 min and blocked for nonspecific binding with phosphate-buffered saline (PBS) supplemented with 10% of goat serum for 30 min. Cells were incubated with specific concentration of dye diluted from stock solution for 1 h. Nuclear DNA was stained with Hoechst 33 342 (Sigma) at 1 : 40 dilution. Cytoplasm was stained with HCS CellMask Cy5 (Invitrogen) at 1 : 20 000 dilution. Actin was stained with Phalloidin 488 (Invitrogen) at 1 : 40 dilution. PBS rinse was conducted three times between each step.

Fluorescent images were collected with a Nikon DS-QiMc camera installed on a customized Nikon TE300 microscope with a 10x Plan Fluor lens (N.A. 0.3, Nikon Melville, NY), a motorized stage, and motorized excitation and emission filters (Prior Scientific, Rockland, MA) controlled by Nikon NIS Elements. Eighty-one (9-by-9 grid) fields of views were consistently generated using the software Nikon NIS-Elements. The size of the image acquired from the camera was 1280 × 1024 pixels, and the pixel size was 0.57 µm for a 10x objective. Our Δ*X* and Δ*Y* for image capture was 662 µm and 520 µm, respectively, to allow 10% overlay between adjacent fields. The total size of the scanning region (81 images) was ~28.5 mm². Four different channels (UV, GFP, Cy5, and phase contrast) were collected for every field of view. The calibration glass-bottom dish contained

dyes for three different fluorescent channels, UV, GFP, and Cy5. For each fluorescence channel, UV, GFP, and Cy5, two calibration images were acquired: with and without illumination. The calibration images were used to reduce the non-uniform illumination of fluorescent images. All of the phenotypic information was calculated with a custom high throughput program (written in Matlab) developed in our laboratory. Typically >1000 cells were analyzed per different biological repeat (*i.e.* different cells) for a total >3000 cells for each tested condition.

Segmentation of cells and nuclei

To precisely segment individual cells and nuclei, we used slightly different approaches based on the same principle. For nuclear segmentation, because of the relatively circular shape and relatively even intensity of the Hoechst stain, we filtered calibrated images (as described in the previous section) with a 23 × 23 pixel normalized Gaussian filter (similar scale as the size of nuclei) and an averaging filter (same size) to obtain I_G (Gaussian intensity) and I_M (averaged intensity). Subtracting I_M from I_G gives I_N , the nuclear intensity values without a regional background. Empirical testing showed that a threshold setting of 10 was optimal.

Because cells are larger than their nuclei, larger size of filters is needed. However, one major limitation with spatial domain image filters is non-continuous edges. Increasing the size of the filter increases the size of this "non-trustable" region. The use of a spatial filter $2r + 1$ in size will lead to the loss of $r + 1$ pixels from the edge because of incomplete information, which greatly reduces the usable image size. For the nucleus, there are only ~12 pixels lost, which is acceptable. For an object the size of the cell, the much larger number of lost pixels is unacceptable. Thus, we did not use any spatial filter to segment individual cells. Rather, images of cells were processed with a 3 × 3 averaging smoothing filter.

To properly threshold single cell boundaries, measurement and elimination of the background intensity of images are more critical. First, we measured the average, $\langle I_{BG} \rangle$, and associated standard deviation, I_{RBG} , of the background intensity of the smoothed image to obtain a set of pixel intensities less than $\langle I_{BG} \rangle + 3.5 * I_{RBG} = I_{nn}$. Then, we update the value of $\langle I_{BG} \rangle$ with I_{nn} , I_{RBG} , and the standard deviation of I_{nn} . Three to five iterations will generally result in stable values of I_{BG} and I_{RBG} , which represent the average background intensity value and associated noise in background intensity magnitude, respectively. Next, we use I_{BG} and I_{RBG} to select the signal region of the fluorescence-labeled cells. We define the threshold factor, thc , and select all the pixels in the image with an intensity value larger than $I_{BG} + thc * I_{RBG}$. We make the assumption that the background noise intensity can be described by a Gaussian distribution and then set $thc > 2$, which represents >95% of the background signal will not be selected. Depending on the signal intensity level, the value of thc will range between 2 and 5.

Using the above approach, we determined the cell boundary using phalloidin-stained F-actin images. F-actin usually gives a stronger signal at the cell boundary than at the cell center,

differentiating the boundary from the cytoplasm with less bias than a more homogenous dye (such as HCS cell mask) would allow for. In fact, HCS cell mask intensities concentrated around the nucleus – the thicker region of the cell – and decayed towards the edge of the cell; because of the low NA objective, the edge intensity values were blurred, making edge detection very sensitive to bias and sample-to-sample variation.

Acknowledgements

The authors thank Dr Jeffrey Stirman and Prof. Gregory D. Longmore for their careful reading of the manuscript.

References

- L. Hartwell and M. Kastan, Cell cycle control and cancer, *Science*, 1994, **266**, 1821–1828.
- J. Folkman and A. Moscona, Role of cell shape in growth control, *Nature*, 1978, **273**, 345–349.
- S. van den Heuvel and E. Harlow, Distinct roles for cyclin-dependent kinases in cell cycle control, *Science*, 1993, **262**, 2050–2054.
- C. J. Sherr, Cancer Cell Cycles, *Science*, 1996, **274**, 1672–1677.
- W. Wang, B. Bu, M. Xie, M. Zhang, Z. Yu and D. Tao, Neural cell cycle dysregulation and central nervous system diseases, *Prog. Neurobiol.*, 2009, **89**, 1–17.
- K. Keyomarsi and A. B. Pardee, Redundant cyclin overexpression and gene amplification in breast cancer cells, *Proc. Natl. Acad. Sci. U. S. A.*, 1993, **90**, 1112–1116.
- C. Jayat and M.-H. Ratinaud, Cell cycle analysis by flow cytometry: principles and applications, *Biol. Cell*, 1993, **78**, 15–25.
- J. V. Harper, *Methods in Molecular Biology*, 2004, vol. 296, pp. 157–166.
- E. A. Klein, L. Yin, D. Kothapalli, P. Castagnino, F. J. Byfield, T. Xu, I. Levental, E. Hawthorne, P. A. Janmey and R. K. Assoian, Cell-Cycle Control by Physiological Matrix Elasticity and *In Vivo* Tissue Stiffening, *Curr. Biol.*, 2009, **19**, 1511–1518.
- B.-J. Benecke, A. Ben-Ze'ev and S. Penman, The control of mRNA production, translation and turnover in suspended and reattached anchorage-dependent fibroblasts, *Cell*, 1978, **14**, 931–939.
- K. Maeshima, K. Yahata, Y. Sasaki, R. Nakatomi, T. Tachibana, T. Hashikawa, F. Imamoto and N. Imamoto, Cell-cycle-dependent dynamics of nuclear pores: pore-free islands and lamins, *J. Cell Sci.*, 2006, **119**, 4442–4451.
- P. H. Wu, S. H. Hung, T. Ren, M. Shih Ie and Y. Tseng, Cell cycle-dependent alteration in NAC1 nuclear body dynamics and morphology, *Phys. Biol.*, 2011, **8**, 015005.
- P. J. Stewart-Hutchinson, C. M. Hale, D. Wirtz and D. Hodzic, Structural requirements for the assembly of LINC complexes and their function in cellular mechanical stiffness, *Exp. Cell Res.*, 2008, **314**, 1892–1905.
- B. R. Johnson, R. T. Nitta, R. L. Frock, L. Mounkes, D. A. Barbie, C. L. Stewart, E. Harlow and B. K. Kennedy, A-type lamins regulate retinoblastoma protein function by promoting subnuclear localization and preventing proteasomal degradation, *Proc. Natl. Acad. Sci. U. S. A.*, 2004, **101**, 9677–9682.
- T. Dechat, T. Shimi, S. A. Adam, A. E. Rusinol, D. A. Andres, H. P. Spielmann, M. S. Sinensky and R. D. Goldman, Alterations in mitosis and cell cycle progression caused by a mutant lamin A known to accelerate human aging, *Proc. Natl. Acad. Sci. U. S. A.*, 2007, **104**, 4955–4960.
- J. B. Moseley and P. Nurse, Cdk1 and cell morphology: connections and directions, *Curr. Opin. Cell Biol.*, 2009, **21**, 82–88.
- K. Polyak, J. Y. Kato, M. J. Solomon, C. J. Sherr, J. Massague, J. M. Roberts and A. Koff, p27Kip1, a cyclin-Cdk inhibitor, links transforming growth factor-beta and contact inhibition to cell cycle arrest, *Genes Dev.*, 1994, **8**, 9–22.
- Z. Darzynkiewicz and G. Juan, *Current Protocols in Cytometry*, John Wiley & Sons, Inc., 2001.
- P.-H. Wu, N. Nelson and Y. Tseng, A general method for improving spatial resolution by optimization of electron multiplication in CCD imaging, *Opt. Express*, 2010, **18**, 5199–5212.
- B. L. Ng and N. P. Carter, Laser excitation power and the flow cytometric resolution of complex karyotypes, *Cytometry, Part A*, 2010, **77**, 585–588.
- R. K. Assoian, Anchorage-dependent Cell Cycle Progression, *J. Cell Biol.*, 1997, **136**, 1–4.
- S. B. Khatau, C. M. Hale, P. J. Stewart-Hutchinson, M. S. Patel, C. L. Stewart, P. C. Searson, D. Hodzic and D. Wirtz, A perinuclear actin cap regulates nuclear shape, *Proc. Natl. Acad. Sci. U. S. A.*, 2009, **106**, 19017–19022.
- D. H. Kim, S. B. Khatau, Y. Feng, S. Walcott, S. X. Sun, G. D. Longmore and D. Wirtz, Actin cap associated focal adhesions and their distinct role in cellular mechanosensing, *Sci. Rep.*, 2012, **2**, 555.
- S. B. Khatau, D. H. Kim, C. M. Hale, R. J. Bloom and D. Wirtz, The perinuclear actin cap in health and disease, *Nucleus*, 2010, **1**, 337–342.
- R. A. Tobey, J. G. Valdez and H. A. Crissman, Synchronization of human diploid fibroblasts at multiple stages of the cell cycle, *Exp. Cell Res.*, 1988, **179**, 400–416.
- W. A. Kues, M. Anger, J. W. Carnwath, D. Paul, J. Motlik and H. Niemann, Cell Cycle Synchronization of Porcine Fetal Fibroblasts: Effects of Serum Deprivation and Reversible Cell Cycle Inhibitors, *Biol. Reprod.*, 2000, **62**, 412–419.
- A. Ballabeni, I.-H. Park, R. Zhao, W. Wang, P. H. Lerou, G. Q. Daley and M. W. Kirschner, Cell cycle adaptations of embryonic stem cells, *Proc. Natl. Acad. Sci. U. S. A.*, 2011, **108**, 19252–19257.
- R. Soni, T. O'Reilly, P. Furet, L. Muller, C. Stephan, S. Zumstein-Mecker, H. Fretz, D. Fabbro and B. Chaudhuri, Selective *In Vivo* and *In Vitro* Effects of a Small Molecule Inhibitor of Cyclin-Dependent Kinase 4, *J. Nat. Cancer Inst.*, 2001, **93**, 436–446.

- 29 C. M. Hale, A. L. Shrestha, S. B. Khatau, P. J. Stewart-Hutchinson, L. Hernandez, C. L. Stewart, D. Hodzic and D. Wirtz, Dysfunctional Connections Between the Nucleus and the Actin and Microtubule Networks in Laminopathic Models, *Biophys. J.*, 2008, **95**, 5462–5475.
- 30 S. B. Khatau, C. M. Hale, P. J. Stewart-Hutchinson, M. S. Patel, C. L. Stewart, P. C. Searson, D. Hodzic and D. Wirtz, A perinuclear actin cap regulates nuclear shape, *Proc. Natl. Acad. Sci. U. S. A.*, 2009, **106**, 19017–19022.
- 31 S. B. Khatau, S. Kusuma, D. Hanjaya-Putra, P. Mali, L. Cheng, J. S. Lee, S. Gerecht and D. Wirtz, The differential formation of the LINC-mediated perinuclear actin cap in pluripotent and somatic cells, *PLoS One*, 2012, **7**, e36689.
- 32 S. B. Khatau, R. J. Bloom, S. Bajpai, D. Razafsky, S. Zang, A. Giri, P. H. Wu, J. Marchand, A. Celedon, C. M. Hale, S. X. Sun, D. Hodzic and D. Wirtz, The distinct roles of the nucleus and nucleus-cytoskeleton connections in three-dimensional cell migration, *Sci. Rep.*, 2012, **2**, 488.
- 33 D. Dorner, S. Vlcek, N. Foeger, A. Gajewski, C. Makolm, J. Gotzmann, C. J. Hutchison and R. Foisner, Lamina-associated polypeptide 2 α regulates cell cycle progression and differentiation *via* the retinoblastoma-E2F pathway, *J. Cell Biol.*, 2006, **173**, 83–93.
- 34 G. Salpingidou, A. Smertenko, I. Hausmanowa-Petrucewicz, P. J. Hussey and C. J. Hutchison, A novel role for the nuclear membrane protein emerin in association of the centrosome to the outer nuclear membrane, *J. Cell Biol.*, 2007, **178**, 897–904.